

## Supporting information

### **Holistic functional biomimetic: A key to make efficient electrocatalyst for water oxidation**

Lizhou Fan,<sup>a</sup> Yuxiang Song,<sup>d</sup> Fan Zhang,<sup>b</sup> Brian J.J. Timmer,<sup>a</sup> Alexander Kravberg,<sup>a</sup>  
Biaobiao Zhang,<sup>a,d\*</sup> Licheng Sun<sup>a,c,d</sup>

<sup>a</sup> *Department of Chemistry, KTH Royal Institute of Technology, 10044 Stockholm, Sweden*

<sup>b</sup> *Division of Surface and Corrosion Science, KTH Royal Institute of Technology, 10044 Stockholm, Sweden*

<sup>c</sup> *State Key Laboratory of Fine Chemicals, Institute of Artificial Photosynthesis, DUT-KTH Joint Education and Research Center on Molecular Devices, Dalian University of Technology (DUT), 116024 Dalian, China*

<sup>d</sup> *Center of Artificial Photosynthesis for Solar Fuels and Department of Chemistry, School of Science and Research Center for Industries of the Future, Westlake University, Hangzhou 310024, Zhejiang, China*

\*Corresponding author Email: [zhangbiaobiao@westlake.edu.cn](mailto:zhangbiaobiao@westlake.edu.cn)

## Methods

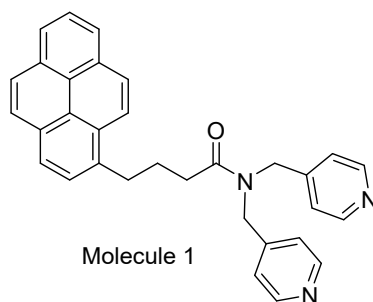
**Materials.** Manganese(II) nitrate hydrate ( $\text{Mn}(\text{NO}_3)_2 \cdot x\text{H}_2\text{O}$ ), 11-aminoundecanoic acid (AUA), sodium hydroxide (NaOH), potassium hydroxide (KOH), hydrogen peroxide ( $\text{H}_2\text{O}_2$ ), hydrochloric acid (HCl), sodium fluoride (NaF), graphene, perchloric acid ( $\text{HClO}_4$ ), and ethanol were purchased from Sigma-Aldrich. The water used for electrolyte was deionized with a Millipore Milli-Q UF Plus system (15-18  $\text{M}\Omega \cdot \text{cm}$  resistivity).

**The preparation of  $\delta\text{-MnO}_2$ .**  $\delta\text{-MnO}_2$  was prepared according to the literature procedure.<sup>[1]</sup> A mixed suspension of 0.6 M NaOH and 2M  $\text{H}_2\text{O}_2$  was quickly poured into a 0.3 M  $\text{Mn}(\text{NO}_3)_2$  solution and stirred for 30 minutes. The precipitate was separated by centrifugation and then transferred into a Teflon autoclave for hydrothermal treatment at 150 °C for 16 h in a 2M NaOH solution. A precipitate was obtained after centrifugation and washing, denoted as  $\delta\text{-MnO}_2$ .

**The exfoliation of  $\delta\text{-MnO}_2$  to  $\text{MnO}_x\text{-NS}$ .** The exfoliation of  $\delta\text{-MnO}_2$  was achieved by the ion exchange and delamination method. Firstly, the  $\delta\text{-MnO}_2$  was immersed in a 0.1 M HCl solution for three days to promote the protonation of  $\delta\text{-MnO}_2$ . Then the sample was soaked in 0.08 M AUA solution with pH 2 for five days, giving AUA- $\delta\text{-MnO}_2$ . The AUA- $\delta\text{-MnO}_2$  was then dispersed in a pH 12 NaOH solution to promote the deprotonation of the carboxylic group of the amino acid molecules. After stirring for one day, the suspension was placed without stirring for another 12 h. After removing the precipitate by centrifugation, the colloidal suspension of exfoliated  $\text{MnO}_x\text{-NS}$  was obtained. The concentration of  $\text{MnO}_x\text{-NS}$  was 12 mg/ml by ICP-OES.

**The preparation of  $\text{MnO}_x\text{-NS/G}$ ,  $\text{MnO}_x\text{-NS/py-G}$ ,  $\delta\text{-MnO}_2\text{/G}$ , and  $\delta\text{-MnO}_2\text{/py-G}$ .**  $\text{MnO}_x\text{-NS/G}$  and  $\delta\text{-MnO}_2\text{/G}$  were prepared by mixing the  $\delta\text{-MnO}_2$  and  $\text{MnO}_x\text{-NS}$  colloidal suspension with a graphene suspension and stirring overnight. For the  $\text{MnO}_x\text{-NS/py-G}$  and  $\delta\text{-MnO}_2\text{/py-G}$ , the pyridine-containing ligand was firstly synthesized with a pyrene anchoring group to get molecule **1**, which was subsequently anchored on graphene via the  $\pi\text{-}\pi$  stacking interaction between graphene and pyrene,

obtaining pyridine modified graphene (py-G).<sup>[2]</sup> Then, MnO<sub>x</sub>-NS and δ-MnO<sub>2</sub> were coupled with py-G via the same procedure to get MnO<sub>x</sub>-NS/py-G and δ-MnO<sub>2</sub>/py-G. The molar ratio of Mn:pyridine functionality during the preparation was adjusted to 7:1.



**Synthesis of the pyridyl molecule.** The pyridyl molecule was prepared by reacting N-(1-pyrene)-butyryloxysuccinimide (Py-Boc) with bis(pyridine-4-ylmethyl)amine.<sup>[3]</sup> A solution of Py-Boc (230 mg, 0.6 mmol) in dry CH<sub>2</sub>Cl<sub>2</sub> (10 mL) was added dropwise to a solution of bis(pyridine-4-ylmethyl)amine (0.119 mg, 0.6 mmol) in CH<sub>2</sub>Cl<sub>2</sub> (10 mL). The resulting mixture was filtered after stirring overnight at room temperature. The filtrate was concentrated under reduced pressure to give a crude product as a yellow solid, which was purified by flash column chromatography on silica gel with MeOH/CH<sub>2</sub>Cl<sub>2</sub> (1:20) as eluent. The desired product was obtained as a white powder (196 mg, 70% yield). <sup>1</sup>H-NMR (400 MHz, CDCl<sub>3</sub>) and ESI-MS (*m/z*) are shown in [Figures S1](#) and [S2](#).

**Reassembly of MnO<sub>x</sub>-NS.** Self-reassembly of MnO<sub>x</sub>-NS was achieved by adding Na<sup>+</sup> into the MnO<sub>x</sub>-NS colloidal suspension.<sup>[4]</sup> The concentration of Na<sup>+</sup> was adjusted to 0.1 M. After ten days, the suspension became colorless and transparent. The precipitate was obtained by centrifugation.

**Physical characterization.** Powder X-ray diffraction (XRD) measurements were carried out on a Bruker D5000 X-ray diffraction diffractometer with Cu K $\alpha$  radiation ( $\lambda = 1.5406 \text{ \AA}$ ). SEM images were obtained with JEOL JSM 7401. TEM images and electron diffraction patterns were taken on a JEOL JEM2100F transition electron microscope. XPS spectra were acquired with a Thermo VG ESCALAB250 surface

analysis system using a monochromatized Al K $\alpha$  small-spot source and a 500  $\mu\text{m}$  concentric hemispherical energy analyzer. All the spectra presented were energy calibrated by setting the adventitious carbon peak to 284.6 eV. The content of the deposited film was analyzed by a Perkin Elmer 2000 DV ICP Optical Emission Spectrometer. UV Vis absorption spectra were measured with a Perkin Elmer Lambda 750 UV-vis spectrophotometer. AFM measurements were carried out using a Bruker Dimension Icon AFM system in air. The tapping mode scan was employed, and Al-coated silicon AFM probes RTESPA-150 from Bruker were used. Images were obtained with a scan rate of 3 Hz and  $512 \times 512$  pixels. The images were subjected to a 3rd order flattening with Nanoscope Analysis v1.5 software, to remove the Z offset, tilting, and bowing. Before AFM measurements, a well-dispersed MnO $_x$  nanosheet solution droplet was deposited on a silica surface and let dry in the air without heating.

**Electrode preparation.** 4 mg of the obtained samples were dispersed in a mixture solution of 768  $\mu\text{L}$  H $_2$ O, 200  $\mu\text{L}$  ethanol, and 32  $\mu\text{L}$  5% Nafion (ethanol solution) by sonication for over one hour. For the glass carbon (GC) electrode, 10  $\mu\text{L}$  of the suspension was drop-casted on the pre-polished GC electrode with surface area of 0.071 cm $^2$  and dried at 50  $^\circ\text{C}$  for 15 mins.

**Electrochemical characterization.** All electrochemical experiments were performed with a CH Instrument 660E potentiostat. The electrochemical cell was equipped with a sample electrode as the working electrode, a platinum foil (2 cm $^2$ ) as the counter electrode, and a standard Ag/AgCl reference electrode. 1 M KOH was used as the electrolyte. All the applied potentials were converted to reversible hydrogen electrode (RHE),  $E \text{ vs. RHE} = E \text{ vs. Ag/AgCl} + 0.059\text{pH} + 0.197 \text{ V}$ , overpotential  $\eta = E \text{ vs. RHE} - 1.23 \text{ V}$ . Linear sweep voltammograms (LSV) were performed with a scan rate of 5 mV s $^{-1}$ . 95 % iR correction was applied with the current interrupt method by the software supplied with the CH Instrument 660E potentiostat. Tafel slope was obtained by plotting overpotential  $\eta$  against  $\log (J)$  from LSV curves. A potentiostat measurement under an overpotential of 450 mV was performed to test the stability of the catalyst. Electrochemically active surface areas (ECSA) were determined by

cyclic voltammetry (CV) at the potential window of 0-0.1 V vs. Ag/AgCl, with different scan rates of 30, 40, 50, 60, 70, and 80 mV/s. By plotting the  $\Delta J = J_a - J_c$  at 0.05 V vs. Ag/AgCl against the scan rate, the linear slope, which is twice the double-layer capacitance ( $C_{dl}$ ), was used to determine ECSA. Electrochemical impedance spectroscopy (EIS) was carried out in the catalytic condition with a frequency ranging from 0.1-10<sup>5</sup> Hz and an applied potential of 1.6 V. Cyclic voltammetry (CV) was operated with a potential range of 0 ~ -1.2 V vs. Ag/AgCl in 0.1 M NaF electrolyte. The pH of the electrolyte was adjusted to 4.7 by 1 M HClO<sub>4</sub>. The Faradaic efficiency was measured in a sealed cell that was purged with N<sub>2</sub>. The actual quantity of O<sub>2</sub> gas evolution was determined by gas chromatography (Shimadzu) every 30 mins. The equation calculated the faradaic efficiency: Faradaic efficiency =  $4F \times n_{O_2} / Q$ , where F is the Faraday constant,  $n_{O_2}$  is the measured O<sub>2</sub> amount, and Q is the consumed charges.

**KIE measurement.** Kinetic isotope effects were studied via electrochemical methods. LSV or CV was recorded at a scan rate of 5 mV s<sup>-1</sup>. For KIE calculation under alkaline conditions, experiments were carried out in NaOH aqueous solution (1.0 M) or NaOD D<sub>2</sub>O solution (1.0 M). For KIE experiments, a pH meter (FiveEasy F20, METTLER TOLEDO) was used for all pH measurements. The pD values were adjusted using NaOD or DCl in accordance with the relation  $pD = pH_{read} + 0.4$ . At least three replicates were performed for KIE measurements at room temperature.

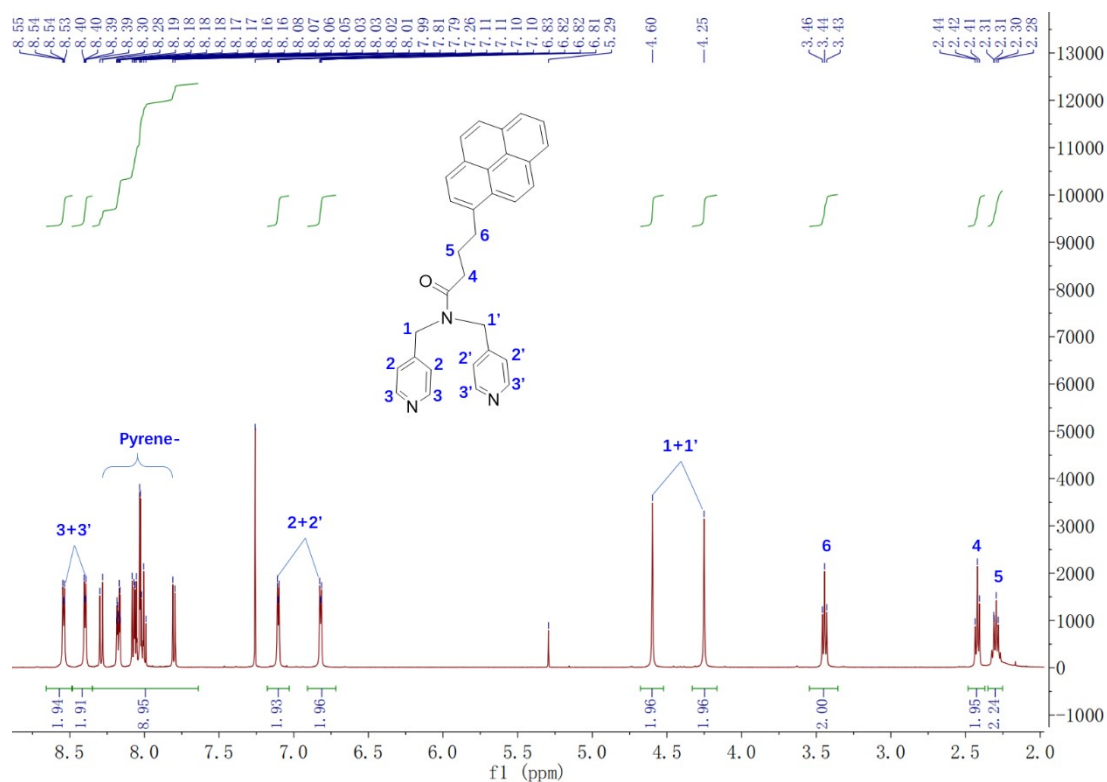


**Figure S1** The  $^1\text{H-NMR}$  (400 MHz,  $\text{CDCl}_3$ ) spectrum of molecule **1**.

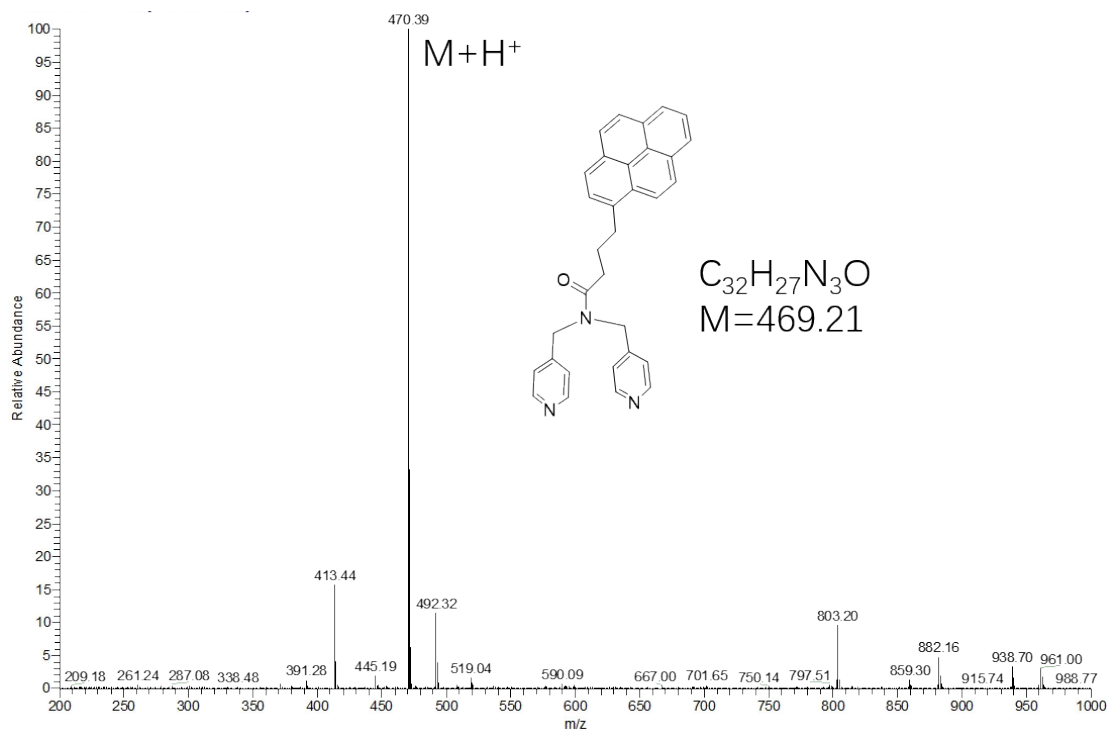


**Figure S2** The ESI-MS ( $m/z$ ) spectrum of molecule **1**.

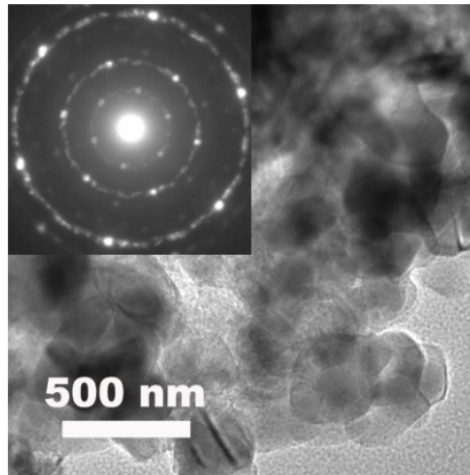


**Figure S3** The TEM and SAED (inset) images of birnessite  $\text{MnO}_x$ .

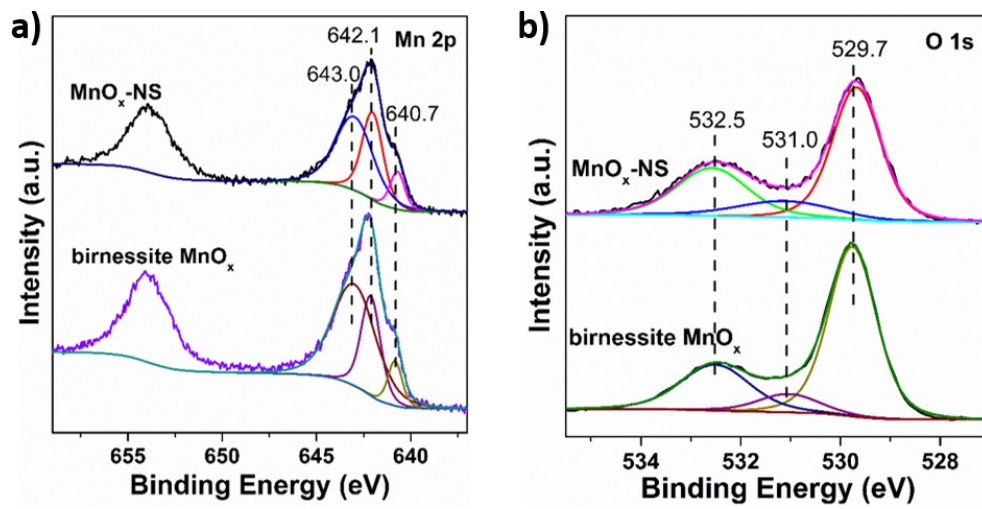


**Figure S4** XPS spectra of birnessite  $\text{MnO}_x$  and  $\text{MnO}_x\text{-NS}$ .

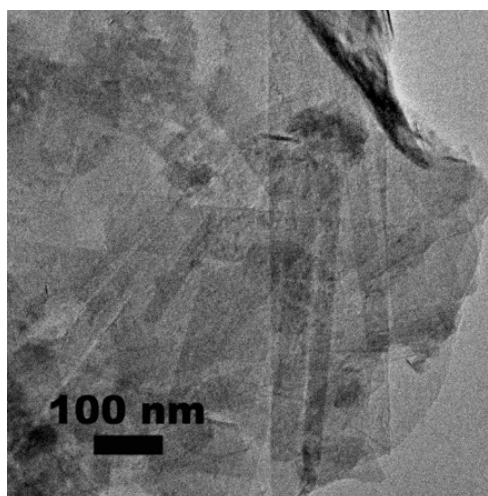


**Figure S5** The TEM image of  $\text{MnO}_x\text{-NS/G}$ .

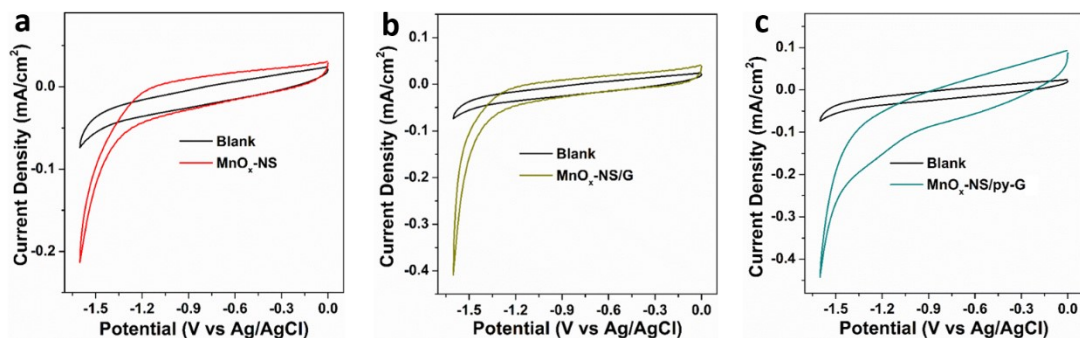


**Figure S6** Cyclic voltammetry at 100 mV/s of a)  $\text{MnO}_x\text{-NS}$ , b)  $\text{MnO}_x\text{-NS/G}$ , and c)  $\text{MnO}_x\text{-NS/py-G}$  in 0.1M NaF electrolyte with pH of 4.7.

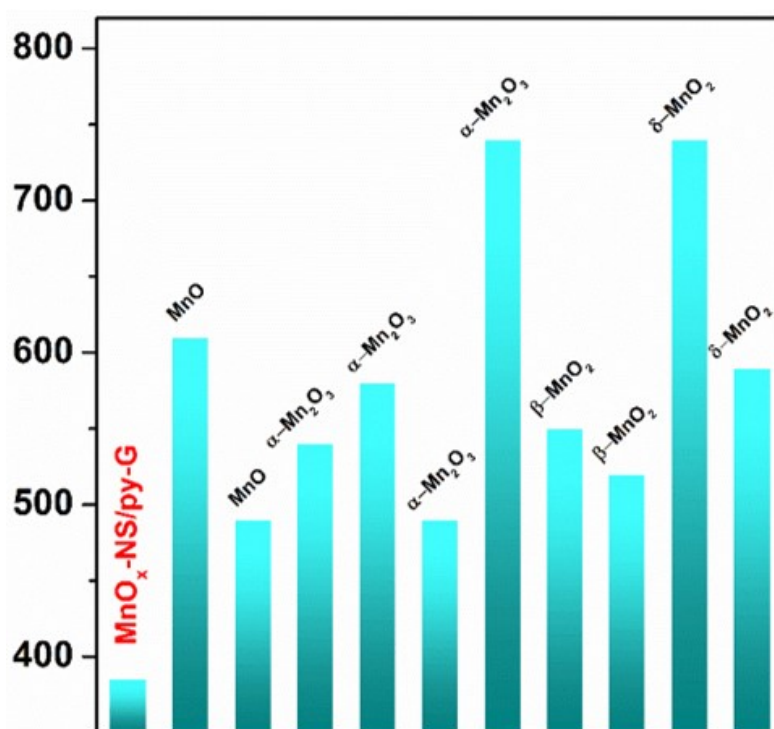


**Figure S7** Comparison of the catalytic performance (overpotential requirement for 10  $\text{mA/cm}^2$  current density) of Mn-based water oxidation catalyst, <sup>[5-11]</sup> note the electrode using Ni foam and carbon fiber paper as the substrate of the electrode is not in this list either because it cannot reflect the intrinsic catalytic activity of the catalyst.

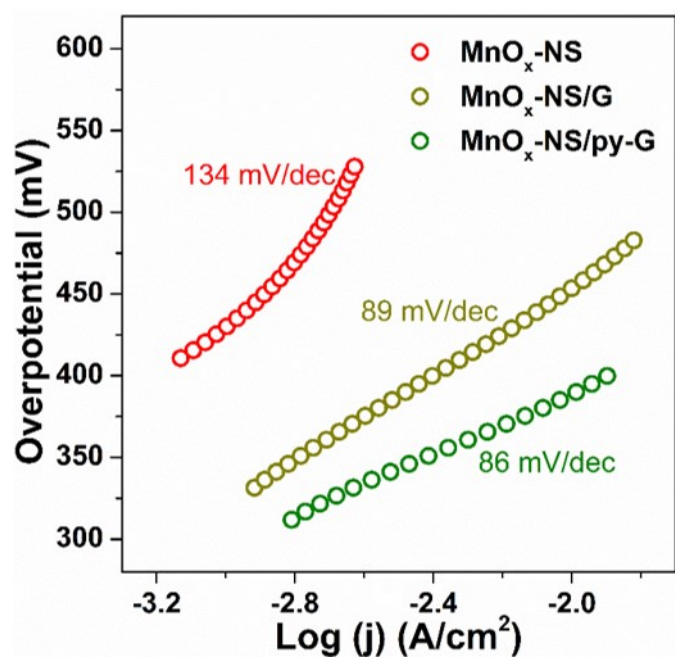


**Figure S8** Tafel slope of MnO<sub>x</sub>-NS, MnO<sub>x</sub>-NS/G and MnO<sub>x</sub>-NS/py-G.

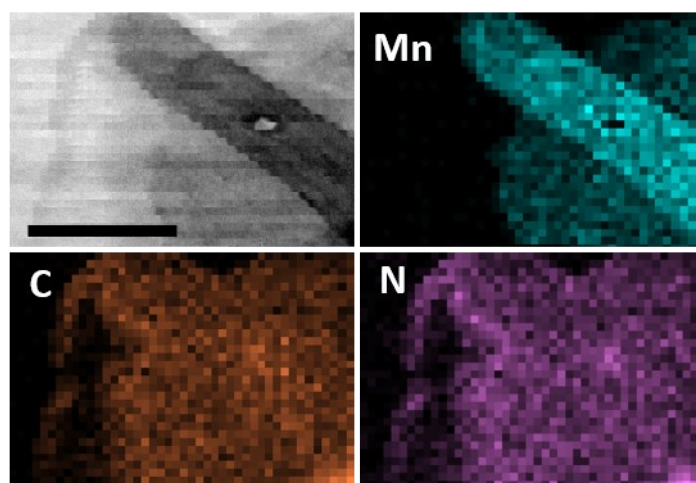


**Figure S9** The TEM image and the STEM-EDX elemental mapping of Mn, C, N of MnO<sub>x</sub>-NS/py-G after catalytic reaction (scale bar is 20 nm).

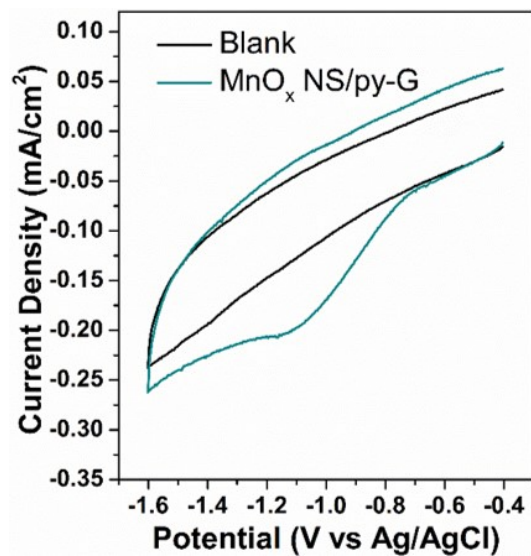


**Figure S10** Cyclic voltammety at 100 mV/s of MnO<sub>x</sub>-NS/py-G after catalytic reaction in 0.1M NaF electrolyte with pH of 4.7.

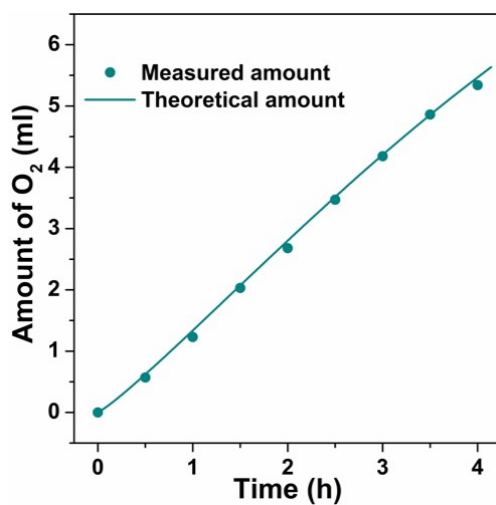


**Figure S11** The experimental and theoretical O<sub>2</sub> evolution amount by electrolysis of MnO<sub>x</sub>-NS/py-G for OER under 400 mV overpotential, evaluated by loading the catalysts on glass carbon (GC) electrodes under alkaline conditions (1 M KOH).

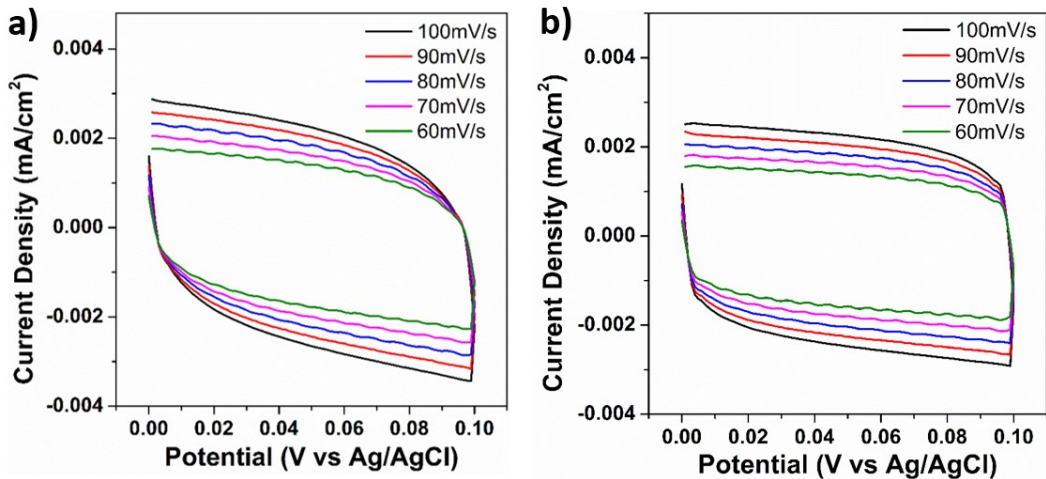


**Figure S12** Cyclic voltammograms of a) birnessite  $\text{MnO}_x$  and b)  $\text{MnO}_x$ -NS in 0~0.1 V (vs. Ag/AgCl) potential range with different scan rates.

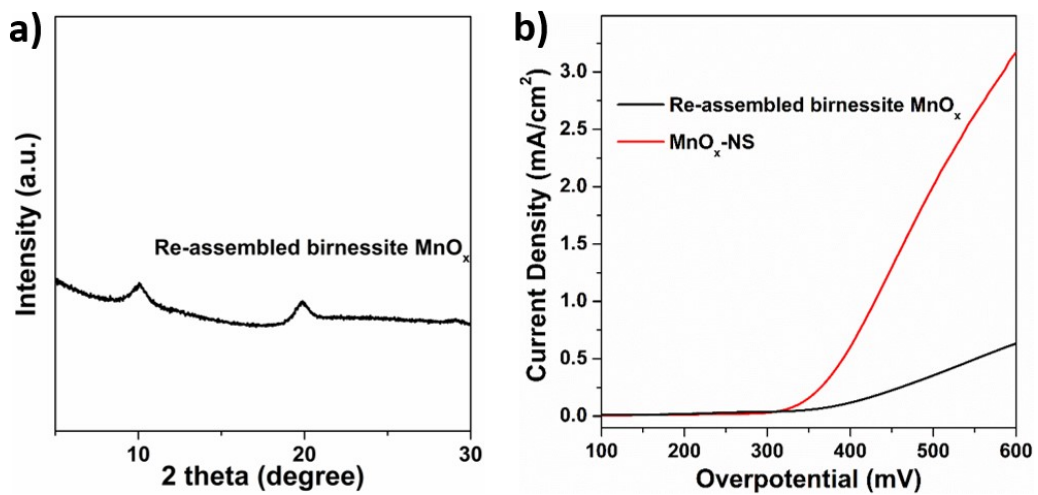


**Figure S13** a) XRD pattern of re-assembled birnessite  $\text{MnO}_x$  from  $\text{MnO}_x$ -NS. b) LSV curves of  $\text{MnO}_x$  NS and re-assembled birnessite  $\text{MnO}_x$ .

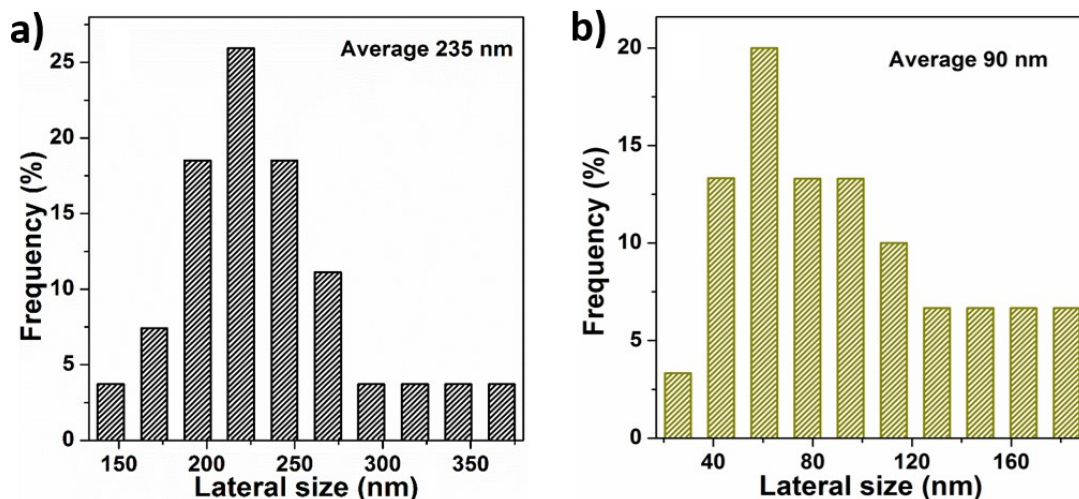


**Figure S14** The lateral size distributions of a) bulk birnessite  $\text{MnO}_x$  and b)  $\text{MnO}_x$ -NS.

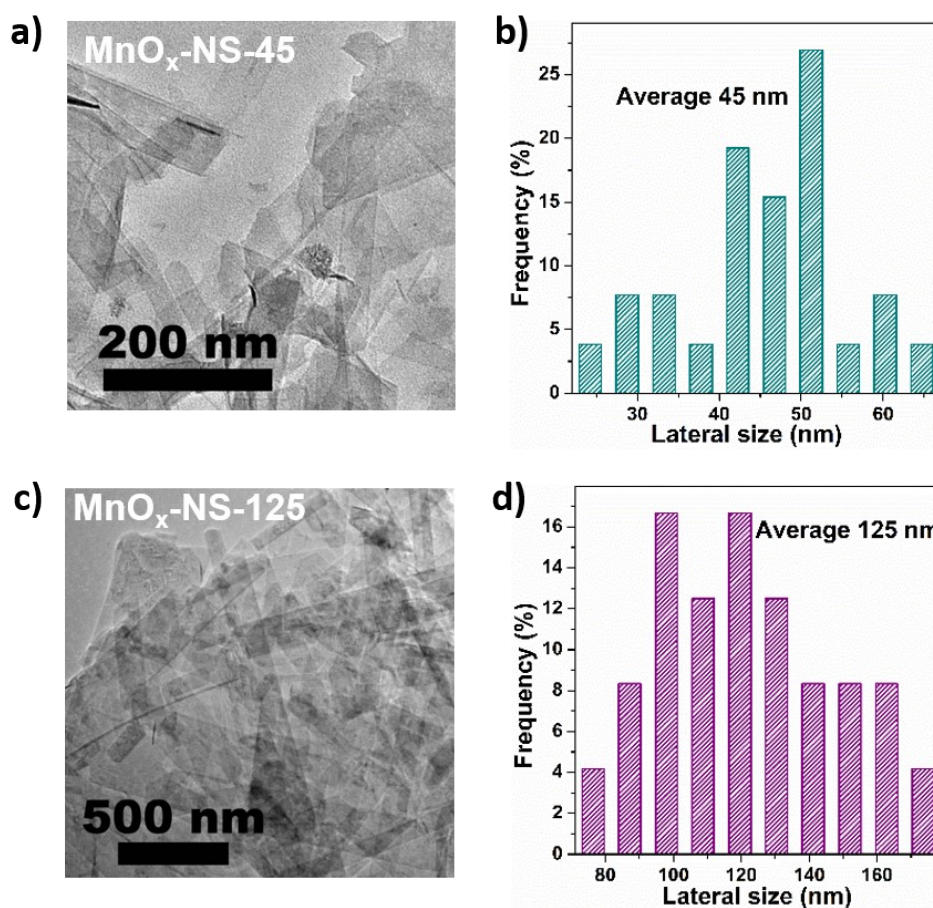


**Figure S15** a) TEM image and b) Size distribution of the lateral size of  $\text{MnO}_x$ -NS-45.

c) TEM image and d) Size distribution of the lateral size of  $\text{MnO}_x$ -NS-125.

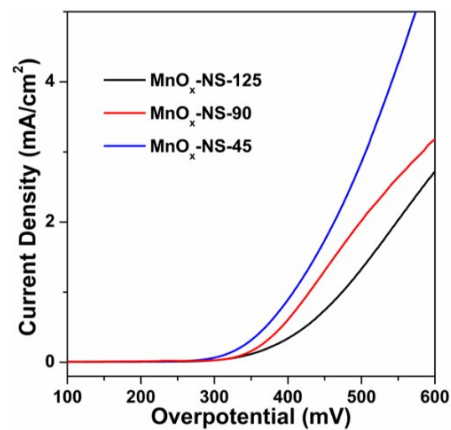


**Figure S16** LSV curves of  $\text{MnO}_x\text{-NS-45}$ ,  $\text{MnO}_x\text{-NS-90}$ , and  $\text{MnO}_x\text{-NS-125}$ .

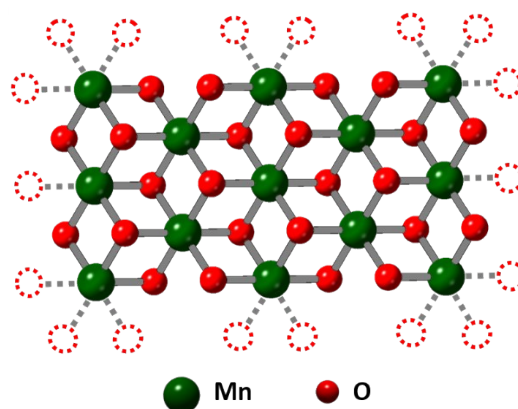


**Figure S17** Corresponding structural illustration of edge- and corner-site-enriched 2D  $\text{MnO}_x\text{-NS}$  with abundant unsaturated coordination sites.

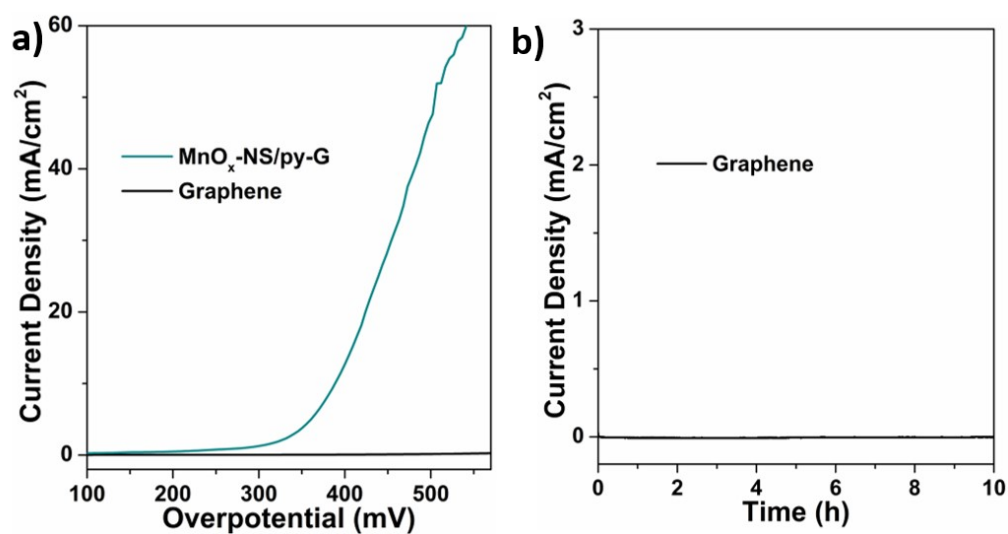


**Figure S18** a) LSV curve comparison of graphene and  $\text{MnO}_x\text{-NS/G}$ . b) Chronoamperometry curve of graphene under 450 mV overpotential.

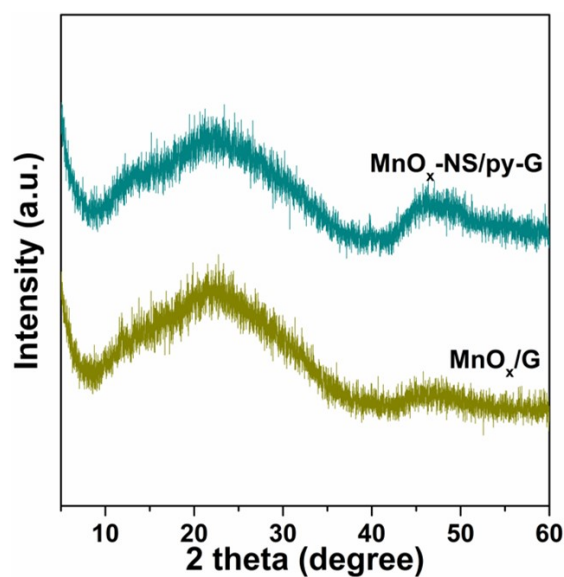


Figure S19 XRD pattern of  $\text{MnO}_x\text{-NS/G}$  and  $\text{MnO}_x\text{-NS/py-G}$ .

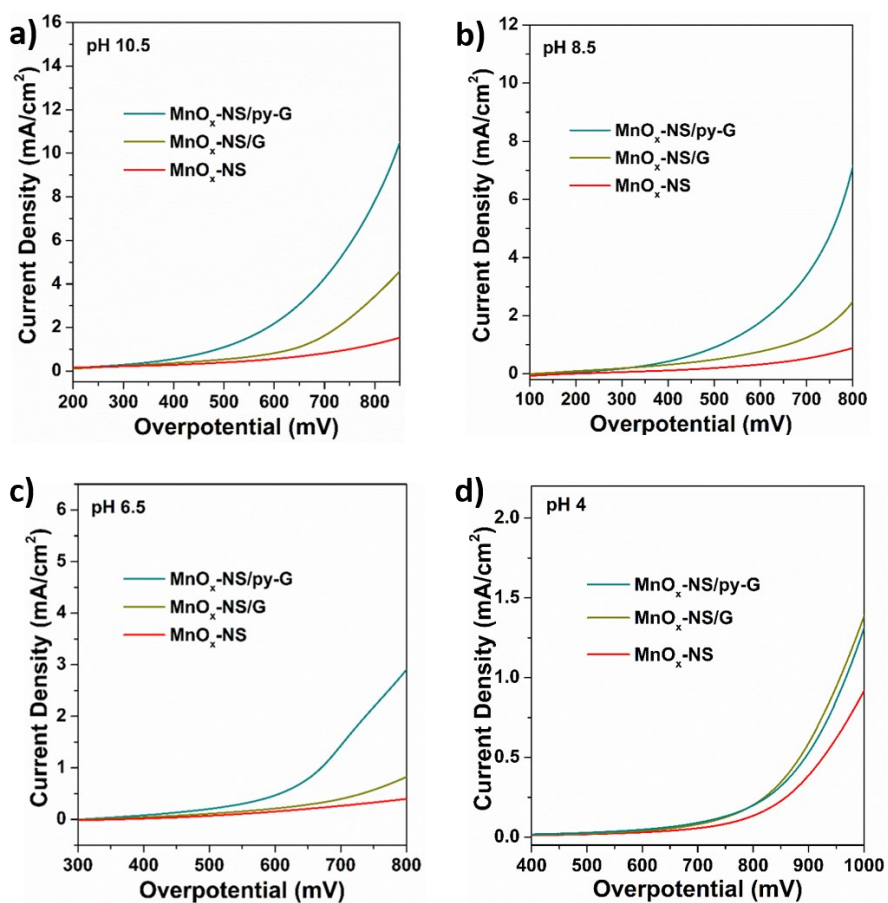
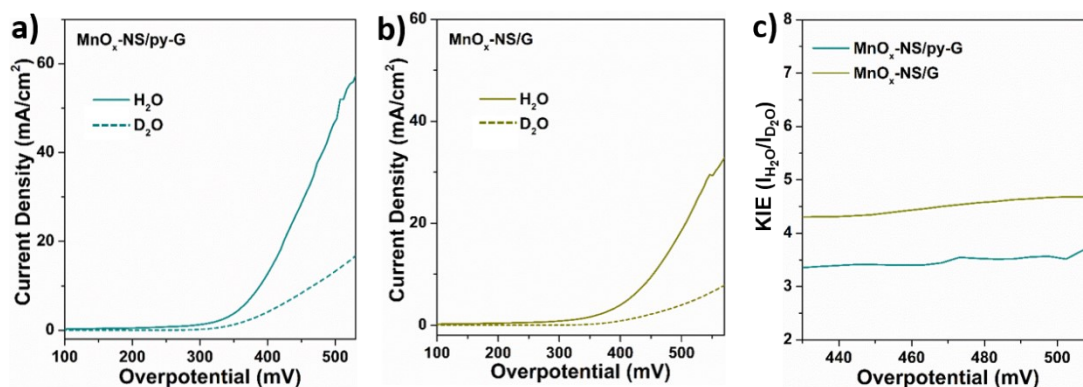


Figure S20 LSV curves of  $\text{MnO}_x$  NS,  $\text{MnO}_x$  NS/G, and  $\text{MnO}_x$  NS/py-G on GCE measured in pH 10.5, pH 8.5, pH 6.5, and pH 4 0.1M PBS electrolyte.



**Figure S21** LSV curves of a)  $\text{MnO}_x$  NS/py-G and b)  $\text{MnO}_x$  NS/G in 1 M KOH  $\text{H}_2\text{O}$  solution and KOD  $\text{D}_2\text{O}$  solution, c) the calculated kinetic isotope effect (KIE) values of  $\text{MnO}_x$  NS/py-G and  $\text{MnO}_x$  NS/G ( $\text{KIE} = I_{\text{H}_2\text{O}}/I_{\text{D}_2\text{O}}$ ).

## Reference

- [1] Feng, Q.; Yanagisawa, K.; Yamasaki, N., *J. Mater. Sci. Lett.*, 1997, **16**, 110-112.
- [2] Liu, J.; Tang, J.; Gooding, J. J., *J. Mater. Chem.*, 2012, **22**, 12435-12452.
- [3] Li, F.; Zhang, B.; Li, X.; Jiang, Y.; Chen, L.; Li, Y.; Sun, L., *Angew. Chem. Int. Ed.*, 2011, **50**, 12276-12279.
- [4] Yang, X.; Makita, Y.; Liu, Z.; Sakane, K.; Ooi, K., *Chem. Mater.*, 2004, **16**, 5581-5588.
- [5] Vermaas, D. A.; Bajracharya, S.; Sales, B. B.; Saakes, M.; Hamelers, B.; Nijmeijer, K., *Energy Environ. Sci.*, 2013, **6**, 643-651.
- [6] Pickrahn, K. L.; Park, S. W.; Gorlin, Y.; Lee, H. B. R.; Jaramillo, T. F.; Bent, S. F., *Adv. Energy Mater.*, 2012, **2**, 1269-1277.
- [7] Fekete, M.; Hocking, R. K.; Chang, S. L. Y.; Italiano, C.; Patti, A. F.; Arena, F.; Spiccia, L., *Energy Environ. Sci.*, 2013, **6**, 2222-2232.
- [8] Walter, C.; Menezes, P. W.; Loos, S.; Dau, H.; Driess, M., *ChemSusChem*, 2018, **11**, 2554-2561.
- [9] Meng, Y.; Song, W.; Huang, H.; Ren, Z.; Chen, S. Y.; Suib, S. L., *J. Am. Chem. Soc.*, 2014, **136**, 11452-11464.
- [10] Gorlin, Y.; Jaramillo, T. F., *J. Am. Chem. Soc.*, 2010, **132**, 13612-13614.
- [11] Pickrahn, K. L.; Gorlin, Y.; Seitz, L. C.; Garg, A.; Nordlund, D.; Jaramillo, T. F.; Bent, S. F., *Phys. Chem. Chem. Phys.*, 2015, **17**, 14003-14011.